Is Actin Filament Sliding Responsible for Endoplasmic Reticulum and Golgi Movement?

Joseph F McKenna[1], Stephen E D Webb[2,3], Verena Kriechbaumer[1] and Chris Hawes[1*]

[1]. Plant Cell Biology, Dept. Biological and Medical Sciences, Oxford Brookes University, Oxford, OX3 0BP

[2]. Central Laser Facility, Research Complex at Harwell, Science and Technology Facilities Council, Rutherford Appleton Laboratories, Oxfordshire OX11 0QX

[3]. Present address; Biotechnology and Biological Sciences Research Council, Polaris House, Swindon, SN2 1UH

*Author for correspondence

chawes@brookes.ac.uk, ORCID ID 0000-0003-4856-7690
josephmckenna@brookes.ac.uk, ORCID ID 0000-0003-4838-6048
Stephen.webb@bbsrc.ac.uk, ORCID ID 0000-0002-6304-1702
vkriechbaumer@brookes.ac.uk, ORCID ID 0000-0003-3782-5834

Summary

In plants, the actin cytoskeleton and myosins are fundamental for normal dynamics of the endomembrane system and cytoplasmic streaming. We present evidence that this is in part due to myosin driven sliding of actin filaments within a bundle which generates the motive force required for cell dynamics *in planta*.

Abstract

In plants both the Golgi apparatus and the endoplasmic reticulum (ER) are highly motile. The Golgi apparatus, consisting of numerous Golgi stacks, is physically tethered to the surface of the motile ER membrane. Evidence is inconclusive as to whether there is a direct interaction between these organelles and the actin cytoskeleton, although there are reports of linker proteins between actin filaments and the ER membrane. Here, we use a combination of fluorescence recovery after photobleaching and a photoactivation strategy to investigate whether myosin driven actin filament sliding is a contributing factor in ER movement and thus Golgi motility. Utilising three different actin binding fluorescent protein constructs we show that recovery of fluorescence after photobleaching and loss of fluorescence after photoactivation is impeded by overexpression of a truncated myosin tail domain known to slow ER movement. We conclude that ER movement is in part mediated by myosin driven sliding of actin filaments within bundles linked to the ER membrane.

Introduction

Many organelles in plant cells display a range of dynamic movements in the cytoplasm. At its simplest these can be divided into two classes. Firstly, classic cytoplasmic streaming, where movement is due to shear forces induced by actomyosin driving larger organelles (Ueda et al., 2010). This can be particularly apparent in *trans*-vacuolar strands of leaves. Secondly, more controlled movement of organelles over the actin cytoskeleton at the cortex of cells, especially in highly vacuolated tissues (Boevink et al., 1998). Even before the advent of live cell imaging based on fluorescent protein technology, it had been shown that in plants the endoplasmic reticulum (ER) network structure (Quader et al., 1989) and Golgi body dynamics (Satiat-Jeunemaitre et al., 1996) are somehow organised by the actin cytoskeleton. By the combination of GFP expression and live cell imaging this organisation is exemplified by the movement of Golgi bodies and ER exit sites (ERES) with the ER network (Boevink et al. 1998, Da Silva et al 2004) and the various different movements of the ER, with four distinct forms having been identified (Runions et al., 2006, Sparkes et al., 2009a, Griffing 2010, Griffing et al., 2017). Both remodelling of the ER and Golgi movement are inhibited by depolymerisation of actin, demonstrating the importance of the actin cytoskeleton (Boevink et al., 1998, Sparkes et al., 2009a).

One possible explanation for these movements is that myosin molecules link the organelles to the actin cytoskeleton and generate the necessary motive force to explain all the observed organelle movements. There are four members of the myosin VIII family, which most likely function as tensors at the cell surface rather than as motors (Ryan and Nebenführ 2018). In arabidopsis there are thirteen members of the myosin XI family most of which display some form of motor activity (Buchnik et al., 2015). The fastest of which reaches up to 50μms^{-1} in

Chara corallina in *in vitro* assays, is significantly faster than mammalian homologues (Higashi-Fujime et al., 1995; Yamamoto et al., 1994).

In higher plant cells, myosin XI motility is up to 5µms^{-1}, an order of magnitude lower than in algae but still 10-fold faster than human myosin Va (Mehta et al., 1999; Tominaga and Nakano, 2012). Mutant knock-out analysis of four members of the XI family (*xi-k, xi-1, xi2* and *xi-i*) demonstrate that these proteins are important for normal whole-organism and cellular growth as well as Golgi body dynamics (Peremyslov et al., 2010). They are also important for normal dynamics of the actin cytoskeleton in planta, with the knockout line showing decreased turnover with a 2-fold reduced filament severing frequency (Cao et al., 2014). Chimeric expression of a slow myosin XI-2, composed of the native myosin XI-2 with the motor domain replaced with *Homo sapiens* myosin Vb motor domain or a fast chimeric myosin protein which contains the *Chara corallina* myosin XI motor domain, results in smaller and larger cell size respectively (Tominaga et al., 2013). This correlation between myosin motility and cell size demonstrates the importance of the actomyosin system in plants.

By over-expression of truncated forms of the myosin XI family in tobacco leaf cells, it was shown that a number of these will inhibit both Golgi and ER movement, presumably by complexing with the native myosin and rendering it non-functional (Avisar et al., 2009, Sparkes et al., 2008). However, despite a number of publications expressing fluorescently tagged myosin constructs of various different forms, there is no convincing evidence of any full length myosins decorating the ER surface or Golgi bodies (Buchnik et al., 2015, Kriechbaumer et al., 2015). It has however been suggested that myosin XI-K associates with endomembrane-derived vesicles in arabidopsis (Peremyslov et al., 2012). DIL domain (homologue of a yeast secretory vesicle binding domain of Myo2p) constructs from arabidopsis myosin XIs locate to various organelles and one from myosin XI-G only labels Golgi and ER (Sattarzaeh et al., 2011). Thus, apart from these few hints, it is still an open question as to how force is generated to induce motility in the two major organelles of the secretory pathway, the ER and Golgi bodies.

Besides the cortical actin cytoskeleton supporting organelle movement, it is dynamic in its own right. Filaments and actin bundles continually remodel in the cytoplasm, and this can involve lateral-filament migration, sliding on actin bundles, filament severing and elongation (Sheahan et al., 2004, Staiger et al., 2009, Henty-Ridilla et al., 2013).

One possible mechanism to explain movements of the cortical ER network is that the motive force comes from motile Golgi bodies attached to the actin cytoskeleton (Sparkes et al., 2008). Golgi bodies associated with ER networks are restricted to curved membrane surfaces in yeast (Okamoto et al., 2012) and higher plants (Hawes et al., 2015). Recently it has been shown that at least two plant reticulons, with ER tubulation properties, interact with the SAR1p GEF, SEC12, part of the machinery that regulates the organisation of COPII components at the ER exit sites (De Craene et al., 2014, Kriechbaumer et al., 2015). It was demonstrated, however, in tobacco leaf cells that if Golgi bodies were disrupted with Brefeldin A, resulting in the reabsorption of Golgi membrane back to the ER, ER motility still persisted (Saint-Jore et al., 2003). It is however possible that a residual matrix of Golgi associated proteins and putative ER tethers (Latijnhouwers et al., 2007, Osterrieder 2012) remains after such experiments and could still remain associated with the actin cytoskeleton during such drug treatments.

Direct contacts between ER and actin have been reported (reviewed in Stefano & Brandizzi 2018). Cao et al., (2016) reported that the SNARE protein SYP73 may act as a linker between the ER, myosin and the actin cytoskeleton. Although an earlier report of the closely related ER SNARE SYP72 suggested that its function was to mark Golgi-ER import sites on the surface of the ER membrane, with no mention of any association with actin or actin binding proteins (Lerich et al., 2012). Likewise a protein of the NETWORKED family, NET 3B has been shown to bridge between the ER and actin bundles (Wang and Hussey 2017).

One possible explanation for some of the observed ER/Golgi motility is that there is no direct connection between actin filaments, myosin and the organelles, even via linker or receptor proteins. Here, using a photobleaching/photoactivation approach, we explore the hypothesis that ER membrane movement may be generated by myosin induced sliding of actin filaments over one another and that a non-motor link between actin filaments and ER membrane could transfer motive force to the ER membrane, perhaps via SNAREs or NET proteins such as SYP73 and NET3B (Cao et al., 2016, Wang & Hussey 2017). We have used three different probes for plant actin, fABD2 (Sheahan et al., 2004, Ketelaar et al., 2004), Lifeact (Reidle et al., 2008, Smertenko et al., 2010) and a GFP tagged anti-actin alpaca nanobody which, when expressed, self-immunolabels the actin cytoskeleton (Rochetti et al., 2014).

Materials and Methods

Plant lines used and chemical treatments

Stably expressing arabidopsis lines used were as follows, p35S::GFP-HDEL p35S::ST-RFP, GFP-fABD2 (Sheahan et al., 2004, Ketelaar et al., 2004), GFP-MAP4 (Marc et al., 1998, Rosero et al., 2013) were grown on ½ Murashige and Skoog salts with MES (Melford laboratories) and 0.8% Phytagel, vernalised for two days at 4°C in the dark and then grown in 16:8 LD conditions for five days. *N. benthamiana* was grown in 16:8 Light:Dark conditions and four-five week old plants were used for transient transformation. *N. benthamiana* transient transformation was performed as described in Sparkes et al., (2006). All fluorophore-labelled marker lines were infiltrated with an optical density at 600nm (OD) of 0.05. p35S::RFP-XI-A and p35S::RFP-XI-K (Avisar et al., 2009) was transformed with an OD of 0.01. Imaging was performed at 3 days post infiltration (dpi). A jasplakinolide stock solution (10mM) in DMSO was diluted to a working concentration of 10 µM in dH_2O. Plant samples were incubated for 1h in jasplakinolide or control (same concentration of DMSO) solutions.

Cloning constructs.

GFP-ActinCB: The Actin-Chromobody® plasmid containing the alpaca actin-antibody gene was obtained from Chromo-Tek (Martinsried, Germany). Primers were ordered from Eurofins MWG Operon (Ebersberg, Germany). Q5 highfidelity DNA polymerase (New England Biolabs, Herts, UK) was used for the polymerase chain reaction (PCR) reaction. The ActinCb-PCR product was cloned into the binary vector pB7WGF2 providing an N-terminal GFP-tag using Gateway® technology (Invitrogen life sciences). For transient expression the construct was transformed into the *A. tumefacians* GV3101 strain under selection for spectinomycin, gentamycin and rifampicin.

mCherry-paGFP: Primer sequences can be found in supplemental table 1. For p35S::mCherry-paGFP-fABD2 primers were designed to amplify paGFP from the p35S::CXN-

paGFP vector (Runions et al., 2006). The N-terminal FRD primer (JM393) was flanked with Gateway attB1 site and the C terminal REV primer (JM394) with a GGSGG amino acid linker overhang. fABD2 was then amplified by PCR using arabidopsis cDNA from five day old seedlings. The N-terminal FRD primer (JM395) consisted of a 22bp overhang composed of the GGSGG linker and last 7nt from paGFP. The C-terminal REV primer (JM392) contained a Gateway attB2 site. These DNA fragments were then fused together using the NEB HiFi Gibson assembly protocol. In order to generate p35S::mCherry-paGFP-Lifeact, paGFP fused to Lifeact was amplified from paGFP using an N-terminal primer (JM393), flanked with a Gateway attB1 site and a C-terminal REV primer (JM401) with an overhang composing a GGSGG linker, Lifeact and an attB2 site. Both constructs were then cloned into Gateway pDONR221 vector using BP clonase and subsequently a 35S promoter driven gateway compatible mCherry N-terminal vector using LR clonase to give p35S::mCherry-paGFP-fABD2 and p35S::mCherry-paGFP-Lifeact. These were then transformed into *A. tumefacians* GV3101 and selected for with Spectinomycin (50µg/ml), Gentamycin 15 µg/ml and Rifampicin 25µg/ml.

Live cell microscopy

Confocal: Imaging was performed on Zeiss 880 or 800 confocal microscopes both equipped with Airyscan detectors and a 100X 1.46NA lens. Samples were mounted on a #1.5 coverslips with dH_2O. Airyscan imaging was performed on the Zeiss 880 using a 5X digital zoom and a 500-550BP and 565LP dual emission filter. An additional 620SP filter was used to block chlorophyll autofluorescence. For GFP and RFP/mCherry imaging, the 488 nm and 561 nm lasers respectively were used for excitation and the frame integration time was 0.13s. For GFP/RFP imaging, line switching was used (halving the frame rate). A minimum timeseries of 240 frames (≥30s) was collected for each FRAP and activation experiment. The FRAP experimental sequence was five pre-bleach image scans followed by 10 bleaching scans with the 488 nm laser at 100% in a square region (160x160 pixels) and then confocal imaging as described above. For photoactivation experiments, the 405 nm laser was used at 50% power for 10 iterations in a similarly square region prior to imaging.

TIRF imaging was performed on a Nikon Ti-E microscope equipped with an iLas2 TIRF FRAP system (Roper), Triline laserbank (Cairn), HQ525/50m emission filter (Chroma) and sCMOS detector (Prime 95B, Photometrics). A 100X 1.46NA lens was used and data was collected using MetaMorph. Excitation and bleaching were performed with a 488nm laser, with FRAP experiments involving 10 iterations of the 488nm laser at full power in the selected region of interest (ROI).

Image analysis

Airyscan processing was performed in Zen Black version 2.1 SP3 14.0.0.0. ROI intensity data was extracted using Zen blue (v2.3). Image editing, kymographs and temporal colour coded projections was performed in FIJI (Image J version 1.51u). Golgi tracking was performed using Trackmate (v3.6.0) (Tinevez et al., 2017). The RFP channel was segmented using a LoG detector with an estimated blob diameter of 1µm, threshold of 10, a medium filter and sub-pixel localisation. All Golgi bodies tracked for fewer than 5 frames were discarded. FRAP analysis was performed as described in Martiniere et al. (2012) with data being normalised and then fit to a non-linear regression one phase association curve. Photoactivation intensity data was normalised in the same way, however a non-linear regression one phase decay curve was fitted. For FRAP and photoactivation data, as well as recovery / decay

curves, $t_{1/2}$ and fluorescence plateau values were calculated. In order to demonstrate actin sliding, the intensities in the activation region and an adjacent region a set distance apart were analysed and normalised to T0 = 100% fluorescence intensity. ANOVA or students T-test were performed depending on the data set. All data was collated in Microsoft Excel. Curve and box-plot generation and all statistical analysis were performed in Graphpad (v7.04). For box plots, blue error bars indicate the standard deviation (SD) and the red line represents mean value. Figures were generated in Adobe illustrator CC (v22.0.1).

Results

Actin cytoskeleton and ER dynamics in the hypocotyl versus cotyledon epidermis

Both the actin cytoskeleton and the Golgi ER/Golgi network display dramatically different dynamics depending on cell and tissue type (Fig.1; videos 1-3). In pavement cells of arabidopsis cotylendonary leaves both the actin cytoskeleton (Fig. 1A-C; video 2) and the ER/Golgi network are motile, whereas in basal cells of the hypocotyl movement is restricted (Fig. 1D; video 1). This can be demonstrated by kymographs of the actin cytoskeleton over a 30s time frame where straight lines indicate little movement in the actin filament network over time (Fig. 1B), and temporal colour coded projections (Fig. 1C). As plant Golgi bodies are attached to and move with the ER network (Da Silva et al., 2004, Osterrieder et al., 2017), their movement can be tracked and also used as a proxy for ER membrane movement. As can be seen in figure 1D-E there is a significant difference between endomembrane dynamics in cotyledon epidermal cells and hypocotyl cells (Fig. 1D and E; video 1). Golgi velocity in cotyledonary and hypocotyl cells were 0.67 ± 0.69µm/s (SD) and 0.33 ± 0.43µm/s (SD) respectively. To assess the movement of individual actin filament bundles, as opposed to rearrangements of the whole actin cytoskeleton, we selectively photobleached cortical regions of the GFP-fABD2 tagged cytoskeleton in cotyledon and hypocotyl cells and measured recovery rates (Fig. 1F and G; video 3). Recovery from bleaching is significantly faster (students T test, $p \leq 0.0001$) in the cotyledon cells, with intensity plateau values at 62 ± 12.89% (SD) compared to 27.8 ± 16.92% (SD, Fig. 1H) in hypocotyl cells. In addition, the halftime of GFP-fABD2 recovery was also significantly decreased (students T test, $p \leq 0.0001$) with cotyledonary cells at 3.5 ± 1.8s (SD) and hypocotyl at 5.9 ± 3.1s (SD) (Fig. 1F-I, video 3). This indicates either a faster growth of actin filaments in cotyledon cells or a faster rate of sliding between filaments in an actin bundle. As recovery appears to be from the edges of the bleached squares, this suggests that this is due to filament sliding rather than turnover of fABD2 on the individual filaments. Interestingly, in both cell types, microtubule dynamics appeared similar (Supplementary Figure 1A) as fluorescence recovery after bleaching was similar in hypocotyls and cotyledon cells (Supplementary Fig S1B-D). Thus it is likely that ER-Golgi dynamics are dependant on actin dynamics and not microtubule activity.

ER tubule elongation moves over existing actin bundles

The cortical ER in cotyledon and mature leaf epidermal cells shows various differing movements including polygon rearrangement, movement of the membrane surface and tubule outgrowths (Sparkes et al., 2009a). To test if the latter was mediated by actin filament polymerisation we transiently co-expressed GFP-fABD2 with the ER marker ssRFP-HDEL and imaged with sub-diffraction-limited resolution using the Airyscan detector (Fig. 2; video 4).

We found no evidence of ER tubules tracking actin filament polymerisation. However, growing tubules could be imaged moving along pre-existing actin bundles (Fig. 2 and video 4, white arrows).

Myosin fragment expression inhibits actin filament sliding

We have previously shown that expression of non-functional myosin XI tail fragments can titrate out myosin function in plant epidermal cells and consequently inhibit movement of Golgi bodies and the endoplasmic reticulum (Sparkes et al., 2008, Avisar et al., 2009). Presumably this functions in a similar manner to Myosin Va tail domain expression which turns Myosin Va into an inactive conformation (Li et al., 2006). However, fragments from several of the 13 myosin XI isoforms, on expression in tobacco leaf cells, had no or negligible effects on endomembrane dynamics. We therefore combined our photobleaching experiments with transient expression of myosin tail fragments in tobacco leaf pavement cells, to assess the potential role of myosins in actin filament sliding within large actin bundles. We decided not to use myosin inhibitor drugs such as BDM or ML-7 as their specificity in plants has been called into question (McCurdy 1999 and Seki et al., 2003). Initially we used Total Internal Reflection Fluorescence (TIRF) microscopy to image actin filaments and bundles with high temporal and spatial resolution. In addition to the previously reported changes in actin cytoskeleton structure in myosin knockout mutant lines (Ueda et al., 2010), we saw that actin filament dynamics are also impaired (Fig. 3A, B) when a dominant negative myosin tail domain (XI-K) is also overexpressed (Fig.3B). Therefore, inhibition of myosins via overexpression of the XI-K tail domain perturbs actin network dynamics. Reductions in actin dynamics and more bundled networks have previously been reported for a triple knockout mutants in arabidopsis (Ueda et al., 2010; Cao et al., 2014). Here we demonstrate that this is phenocopied in *N. benthamiana* with transient expression of a dominant negative myosin tail domain (Fig. 3). In order to determine in more detail how fluorescence recovery occurs, we performed Fluorescence Recovery After photobleaching (FRAP) experiments on the TIRF microscope. This recovery occurs along existing filaments (Fig. 3C), but not uniformly, as one would expect if recovery was due to new binding of GFP-fABD2 along the entire length of the filament. For actin labelled with fABD2-GFP and imaged using confocal microscopy, recovery after photobleaching was significantly impeded when myosin XI-K tail fragments were transiently expressed in the leaves (Fig. 4A; video 5). Control plateau and $t_{1/2}$ values were 59.55 ± 17.7% (SD) and 4.6 ± 2s (SD) compared to XI-K values of 44.4 ± 17.6% (SD) and 6.1 ± 3.2s (SD) respectively (Fig. 4B-D) ($p \leq 0.0001$ for plateau, $P \leq 0.001$ for $t_{1/2}$, ANOVA). On expression of a tail fragment of myosin XI-A, previously shown not to inhibit mitochondria movement (Avisar et al., 2009) and ER remodelling (Griffing et al., 2014), there was no significant effect on fluorescence recovery. Therefore, the observed effects with XI-K are not due to unspecific expression of any tail domains (XI-A), but only those which also inhibit endomembrane dynamics (XI-K). This demonstrates that myosins contribute toward the recovery of fluorescence by supporting inter-filament sliding. Photobleaching was performed on the reporter GFP-Lifeact in combination with XI-K tail domain expression (Supplementary Fig. S3A-D) and the intensity plateau level was significantly reduced between the control and XI-K, and between XI-A and XI-K (Supplementary Fig. S3C). The $t_{1/2}$ values for Lifeact photobleaching were not significantly different between the control and, XI-K or XI-A. However Lifeact has previously been shown to recover quickly after FRAP, due to rapid on-off binding of the probe, which could account for the difference in $t_{1/2}$ for Lifeact. To summarise,

in two different actin marker lines, expression of the inhibitory tail domain of XI-K reduces actin dynamics.

Similar experiments were carried out on the actin cytoskeleton in cotyledon epidermal cells self-immunolabelled by transient expression of an alpaca chromobody against actin (Rochetti et al., 2014) and tagged with the gene for GFP (Fig. 5). Inhibition of fluorescence recovery after bleaching in the presence of myosin XI-K was not as dramatic as with fABD2-GFP labelled actin but still significant (Fig. 5 B-D). Plateau values were 70.9 ± 8.5% (SD) for the control and 62 ± 18.47% (SD) for XI-K, which is a statistically significant difference ($p \leq 0.0001$, ANOVA, Fig 1B and C). The $t_{1/2}$ values were 1.8 ± 0.8s (SD) for control and 2.4 ± 2.346s (SD) for XI-K, also a statistically significant difference ($p \leq 0.05$, ANOVA, Fig. 1D). These results were as expected as we have previously shown that expression of this construct in both tobacco and arabidopsis leaves slowed the dynamics of the endomembrane system (Rochetti et al., 2014).

As a further control we measured fluorescence recovery of actin bundles after treatment with jasplakinolide. Jasplakinolide has previously been used *in planta* to stabilise actin filaments (Mathur et al., 1999, Sampathkumar et al., 2011). It also induces actin polymerisation, resulting in the depletion of available G-actin in the cell and therefore inhibiting subsequent polymerisation (Bubb et al., 1994, Bubb et al., 2000). Jasplakinolide treatment did not significantly alter the recovery period, plateau or $t_{1/2}$ of GFP-fABD2 labelled actin filament bundles (Fig 6A-D), indicating that recovery was not due to actin filament polymerisation into the bleached zone. This was the same for the GFP-actinCB after jasplakinolide treatment (Supplementary Fig. S6A-D), with no statistically significant difference in plateau level or $t_{1/2}$. However, there was a significant decrease in Golgi velocity on treatment with the drug (Fig. 6E), although at this stage we have no information as to whether this reflects on a secondary effect of the treatment. It should also be noted that, while significantly slower, Golgi bodies did move. As Golgi body mobility is driven by the actin cytoskeleton, we would expect no Golgi movement if it was completely stabilised. Furthermore, while FRAP recovery was not significantly different between control and jasplakinolide-treated cells, actin cytoskeleton network structure was altered and this could account for the reduction in Golgi body mobility (Fig. 6A).

Alongside the photobleaching experiments, we confirmed our results by transiently expressing fABD2 or Lifeact linked to fused mCherry and photoactivatable-GFP (paGFP) constructs. By dual labelling the actin marker, we can image the entire network using mCherry while imaging the dispersal of activated paGFP. In this way, it was possible to quantify the dispersal of the activated GFP along actin filaments (Fig.7A and B, arrows; video 6). On activation of mCherry-paGFP constructs, the green fluorescence signal rapidly disperses laterally over the mCherry labelled filaments (Fig. 7A; video 6). Measuring the intensity increase of an adjacent ROI a set distance from the activated region, an increase in GFP fluorescence occurred above the initial activation level after T0 (Fig. 7B). This confirms that we are imaging actin filament sliding, as a portion of the activated paGFP has moved out of the activation region and into the adjacent region. Both the plateau value and $t_{1/2}$ of the activated ROI are significantly higher when expressed with XI-K than in the control or XI-A (control plateau: 5.9 ± 5.7% (SD), XI-K plateau 11.3 ± 13.4% (SD),Fig. 7D, control $t^{1/2}$ 3.1 ± 1.3s (SD), XI-K $t^{1/2}$ 5.1 ± 3.5s (SD), Fig. 7E). XI-A photoactivation was similar to the control, thereby demonstrating the specificity of XI-K expression to filament recovery. In addition mCherry-

paGFP-Lifeact activation showed a slower $t_{1/2}$ when expressed with XI-K than in the control or XI-A condition (Supplementary Fig. S4). Therefore, activated paGFP labelled actin moved more slowly out of the ROI when XI-K was expressed, again demonstrating sliding of actin filaments within actin bundles is regulated by myosins.

Discussion

Difference in organelle dynamics between different tissue types

We have demonstrated that the dynamics of the actin cytoskeleton and ER are different between the cotyledon and hypocotyl cells in arabidopsis (Fig.1). Differences in actin filament severing frequency have previous been reported (Li et al., 2015). However, here we have correlated actin cytoskeleton tissue-specific differences with changes in ER remodelling, as Golgi body mobility is also significantly different in these two tissue types. Furthermore, photobleaching of GFP-fABD2 labelled actin demonstrates that the recovery of fluorescence occurs along existing filaments. This raises the possibility that, in addition to previously reported changes in severing rates, actin filament sliding rates might also be different between these two tissue types. If filament sliding is responsible for ER remodelling and thus Golgi motility, these tissue specific differences support our conclusions below on filament sliding in cotyledon epidermal cells.

Myosins are responsible for actin filament sliding

There are a number of ways in which the actin cytoskeleton can support movement within eukaryotic cells, including the interaction between myosin motors, organelles and actin filaments; the rapid polymerisation of actin filaments and the myosin-driven sliding of actin filaments over each other within actin bundles. Plant myosins are now well documented and have long been known to support cytoplasmic streaming in a wide range of cells (Peremyslov et al., 2008). However, regarding the secretory pathway, the role of actin in the dramatic remodelling of the cortical ER network (Quader et al., 1998, Sparkes et al., 2009, Ueda et al., 2010, Griffing et al., 2014), the movement of individual Golgi stacks (Satiat-Jeunematire et al., 1996, Boevink et al., 1998, Nebenführ et al., 1999, Osterrieder et al., 2017) has been the subject of a number of reports. It has also been noted that Golgi bodies probably move in concert with the moving bounding membrane of the ER (DaSilva et al., 2004, Runions et al., 2006). Although it is clear that members of the myosin XI family are involved in such movements (Avisar et al., 2008, 2009, Griffing et al., 2014, Buchnik et al., 2015), there is no convincing evidence for direct endomembrane organelle-myosin-actin interactions, with the exception that myosin XI-K constructs may label some post-Golgi compartments in roots. It was also suggested XI-K labelled ER derived vesicles in leaves with some ER labelling (Peremyslov et al., 2012). In a quadruple myosin mutant knockout line, the actin cytoskeleton structure is altered in addition to organelle dynamics being perturbed (Peremyslov et al., 2010). Additionally, fluorescently tagged, myosin XI-K labels the actin cytoskeleton preferentially to post-Golgi compartments, as determined by co-localisation with a range of marker lines (Peremyslov et al*.,* 2010).

Here we initially demonstrate that new ER tubule formation occurs predominantly along existing actin bundles (Fig. 2.) We then used photobleaching and photoactivation to

determine if myosin driven actin filament sliding occurs. The interpretation of fluorescence recovery data from fluorescent protein-tagged actin networks in plants can be fraught with problems. Both the commonly used fABD2 and Lifeact constructs bind to actin filaments and are subject to on and off turnover on the filaments themselves (Van der Honing et al., 2011). Thus, data from bleaching experiments can either be interpreted as a measurement of turnover of the actin binding fragments or movement/recovery of the actin filaments/bundles themselves. To mitigate this problem, we also utilised actin labelling by the expression of a cameloid actin nanobody spliced to GFP. This results in self-immunolabelling *in vivo* of the actin network (Rochetti et al., 2014). Being an antibody fragment, it can be assumed that the turnover rate of the antibody on the actin filaments will be very low. The results obtained where the same as those with the classic actin markers Lifeact and fABD2, therefore demonstrating that myosin perturbation affects the recovery of fluorescence. This further supports the hypothesis that myosin drives filament sliding within actin bundles. In addition, jasplakinolide stabilises the actin cytoskeleton and depletes the pool of G-actin thereby not allowing subsequent polymerisation. After jasplakinolide treatment, we do not see an effect on photobleaching recovery of fluorescently labelled actin (Fig. 6), which is further evidence that the recovery we are observing is due to myosin driven filament sliding and not polymerisation. Furthermore, while there is a reduction in Golgi body velocity after jasplakinolide treatment, they are still moving. Therefore, if cytoskeleton FRAP recovery still occurs and Golgi bodies are still mobile this implies that myosin driven filament sliding contributes to their mobility and hence ER remodelling. In parallel, we have also employed photoactivatable constructs to label the cortical actin cytoskeleton, which report on the movement of activated fluorescence *and* the actin network simultaneously, not the turnover of the constructs on the filaments. This photoactivation strategy clearly demonstrates movement of fluorescence (and hence bound actin) out of the activated regions into adjacent ones, therefore demonstrating filament sliding.

Utilising the photobleaching and activation strategy our results suggest that the cortical actin filaments within bundles are sliding over each other powered by one or more myosins. To support movement of the ER and Golgi bodies attached to it, it would be necessary to anchor the ER membrane to underlying actin filament bundles. Several recent reports have suggested that SNARE proteins (SYP 73, Cao et al., 2016) and members of the NETWORKED family, NET3b over the ER (Wang and Hussey., 2017) and NET3c at ER-plasma membrane contact sites (Wang et al., 2014), may perform this role. Myosin regulation of actin network structure has been reported previously, with the mammalian myoX motor function being critical for actin reorganisation at leading edges, resulting in filopodia formation (Tokuo et al., 2007). In addition, the mammalian myosin1c stabilises ER sheets via regulating actin filament array organisation (Joensuu et al., 2014). Furthermore, it has been demonstrated *in planta* that myosins are responsible for generating the force required for buckling and straightening of both individual filaments and bundles (Cao et al., 2014). Elegant work using optical tweezers has also demonstrated a role for myosin in actin entry into generated cytoplasmic protrusions (van der Honing et al., 2009). Both of these *in planta* observations hypothesized that myosin facilitated sliding of filaments could account for this, which our work demonstrates.

We propose a new model that both ER and Golgi movement are partly made through the myosin driven sliding of actin filaments within actin bundles that underlie and are anchored to the ER (Fig. 8). This model can account for differences in speeds of ER and Golgi movement

by myosin motors and actin filaments acting either independently or synergistically with each other to induce a range of different speeds of sliding, resulting in differential movement of the filaments attached to the ER. Indeed this model could also explain the differences in cell size observed when expressing fast and slow chimeric myosins (Tominaga et al., 2012) as these would result in respectively increased and reduced filament sliding and cytoplasmic streaming, hence larger and smaller cells. It can also explain the perturbed actin cytoskeleton observed in triple and quadruple mutant knockout lines (Ueda et al., 2010, Peremyslov et al., 2010, Cai et al., 2014). Furthermore, if there are different polarities of actin filaments within a bundle then directionality of ER membrane and associated organelle movement can be controlled in this manner.

Acknowledgements

We thank Dr Mark Fricker for helpful discussions and Dr Frances Tolmie for useful comments on the manuscript. We thank the Oxford Brookes Bioimaging unit for financial support. Access to the TIRF iLas system was provided under an STFC facility access grant to JM and SW (16230034).

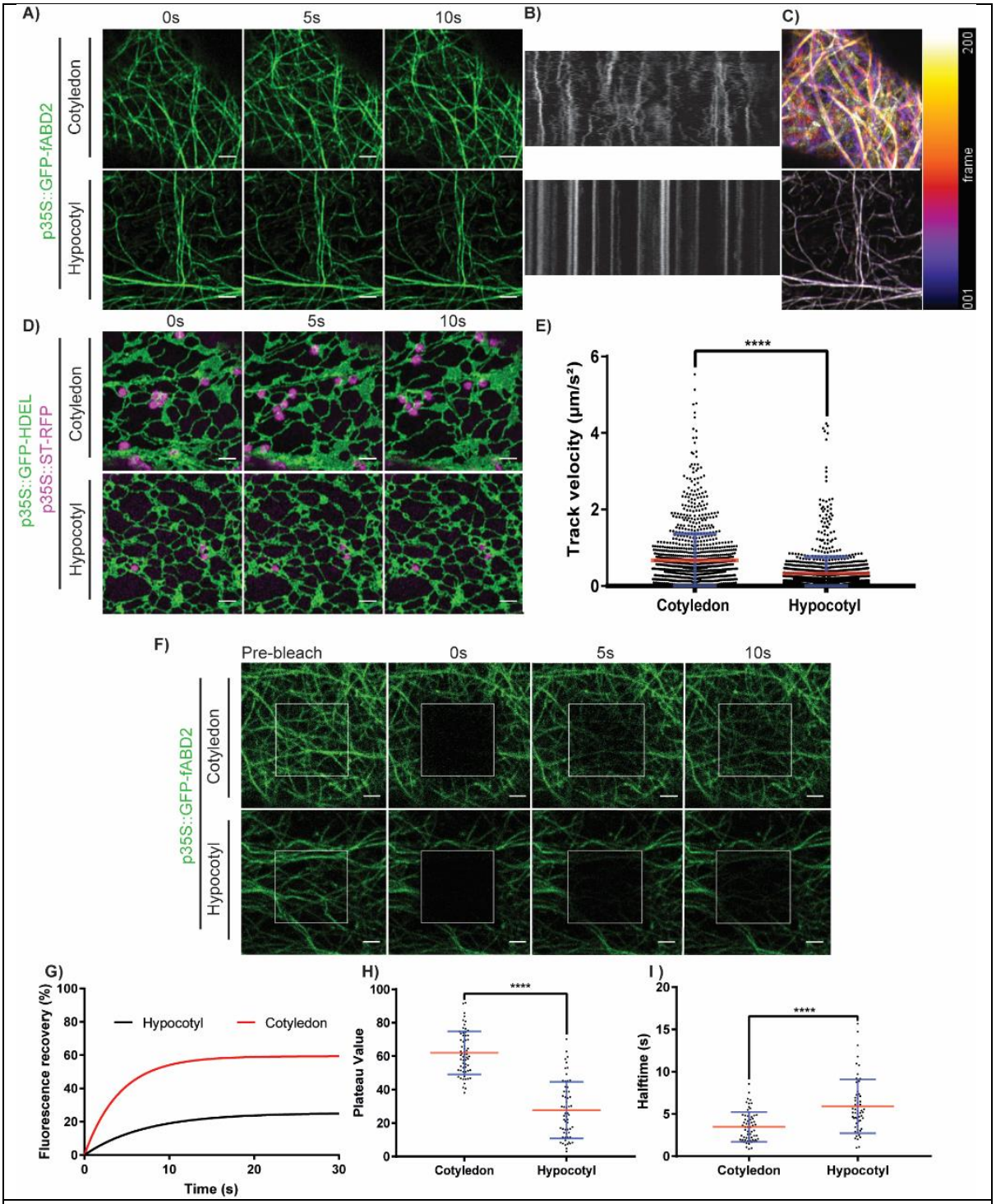

Figure 1. Actin cytoskeleton and ER dynamics differ between hypocotyl and cotyledon tissue in arabidopsis. A) GFP-fABD2 labelled cytoskeleton in the hypocotyl and cotyledon of 5 day old arabidopsis seedlings. N=35 cells across 3 experimental repeats. B) Representative kymographs of GFP-fABD2 over 30s in cotyledon and hypocotyl cells. C) Representative temporal colour coded projections of GFP-fABD2 over 30s in cotyledon and hypocotyl cells. D) GFP-HDEL and ST-RFP labelled 5 day old arabidopsis seedlings in the cotyledon and hypocotyl. N=20 cells across 2 experimental repeats. E) Golgi body tracking in cotyledon and hypocotyl cells. N = 20 cells across 2 experimental repeats. 1286 Golgi bodies tracked for cotyledon, 1338 for hypocotyl. F) FRAP image sequence, G) fluorescence recovery curve, H) plateau value and I) half-time of fluorescence recovery

from GFP-fABD2 in cotyledon and hypocotyl cells. N=62 cells for cotyledon, 57 for hypocotyl, across 2 biological repeats. Students T-test performed, **** = p≤0.0001. Scale bar = 2µm.

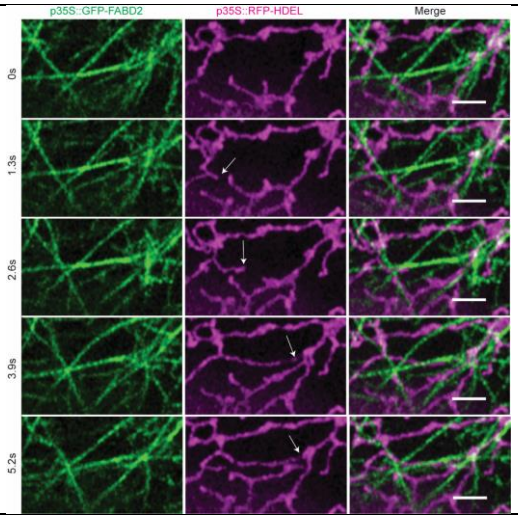

Figure 2. Airyscan imaging of an endoplasmic reticulum tubule elongating over existing actin filaments in *N. benthamiana*. N = 60 cells across 3 experimental repeats. Representative images shown. White arrows showing growing ER tubule. Scale bar = 2µm.

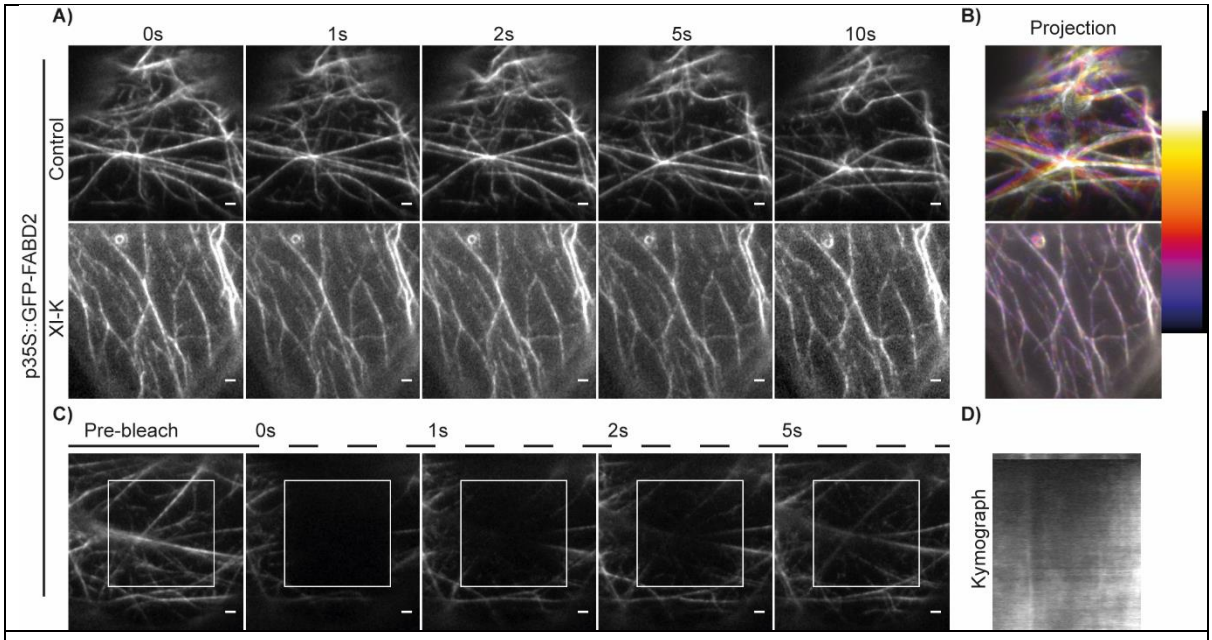

Figure 3. TIRF imaging and transient expression in *N. benthamiana* demonstrates dominant negative myosin XI-K tail domain perturbs actin dynamics *in planta*. A) TIRF Time course data from labelled GFP-fABD2 control and with p35S::RFP-XI-K. N=20 cells, representative images shown. B) Temporal colour coded projection of time-course data in A). C) Fluorescence recovery from the actin cytoskeleton labelled with GFP-fABD2 occurs along existing filaments. N=30 cells, representative images shown. D) Kymograph showing FRAP recovery along actin filament occurs from either side of the bleach region. Scale bar = 2µm.

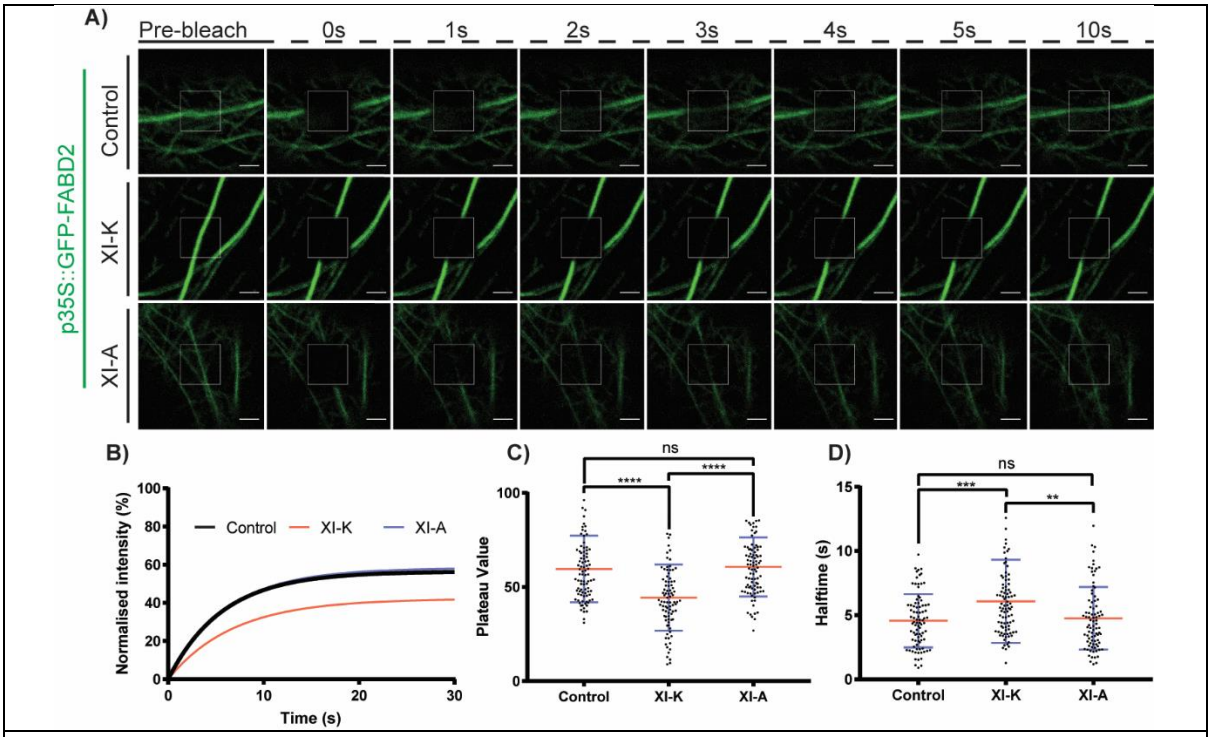

Figure 4) Inhibition of myosin via overexpression of a dominant negative tail domain reduces GFP-fABD2 labelled actin FRAP recovery in *N. benthamiana*. A) Time-course of confocal FRAP showing fluorescence recovery of GFP-fABD2 and co-expression with the dominant negative p35S::RFP-XI-K tail domain. The XI-A tail domain had no effect on ER remodelling or Golgi mobility and so was used as a negative control. B) Fluorescence recovery curves, C) plateau values, D) halftimes of fluorescence recovery for GFP-fABD2 FRAP from control, XI-K and XI-A treatment. For boxplots, error bars (blue) denote standard deviation, mean value (red) is shown. ANOVA statistical analysis was performed. ns = p≥0.05, **=p≤0.01, ***=p≤0.001, ****=p≤0.0001. N=90 cells, across 3 experimental repeats. Scale bar = 2µm.

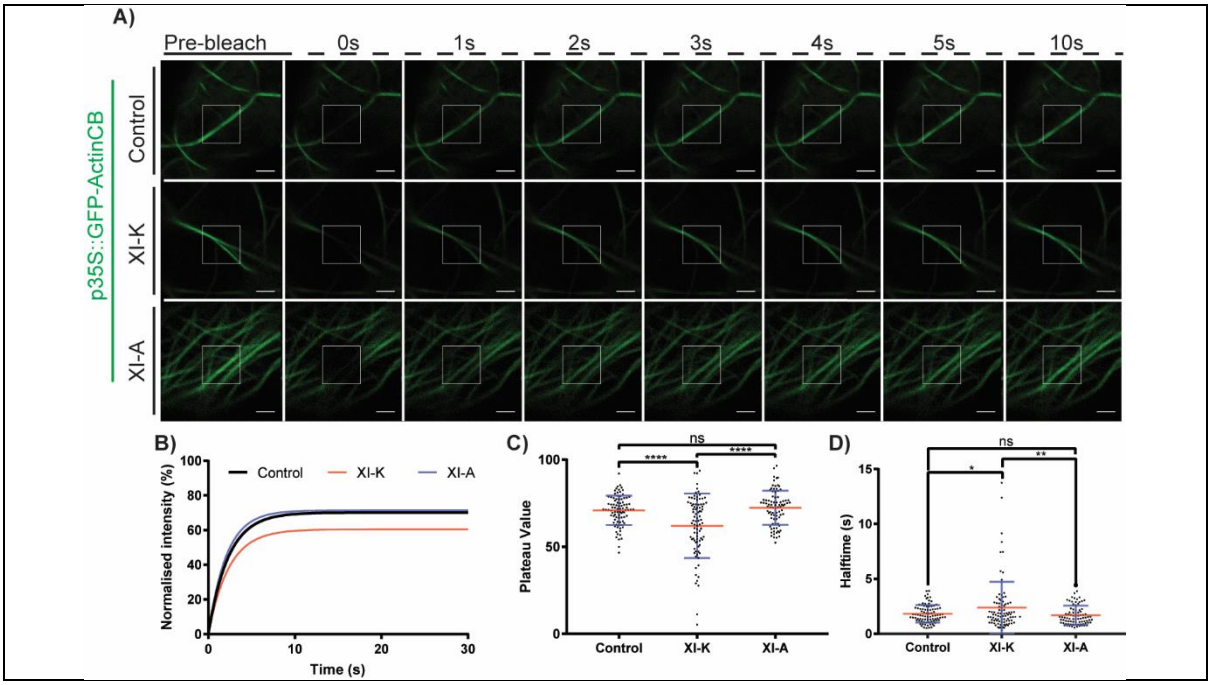

Figure 5) Inhibition of myosin reduces actin FRAP of a self-labelled actin chromobody in *N. benthamiana*. A) Time-course data showing recovery of GFP-actin chromobody (CB) and co-expression with the dominant negative p35S::RFP-XI-K tail domain and the control p35S::RFP-XI-A construct. B) Fluorescence recovery curves, C) plateau values and D) half-times of fluorescence recovery for GFP-fABD2 FRAP from control, XI-K and XI-A treatment. For boxplots, error bars (blue) denote standard deviation, mean value (red) is shown. ANOVA statistical analysis was performed. ns = p≥0.05. *=p≤0.05, **=p≤0.01, ****=P≤0.0001. N=≥85 cells, across 3 experimental repeats. Scale bar = 2µm.

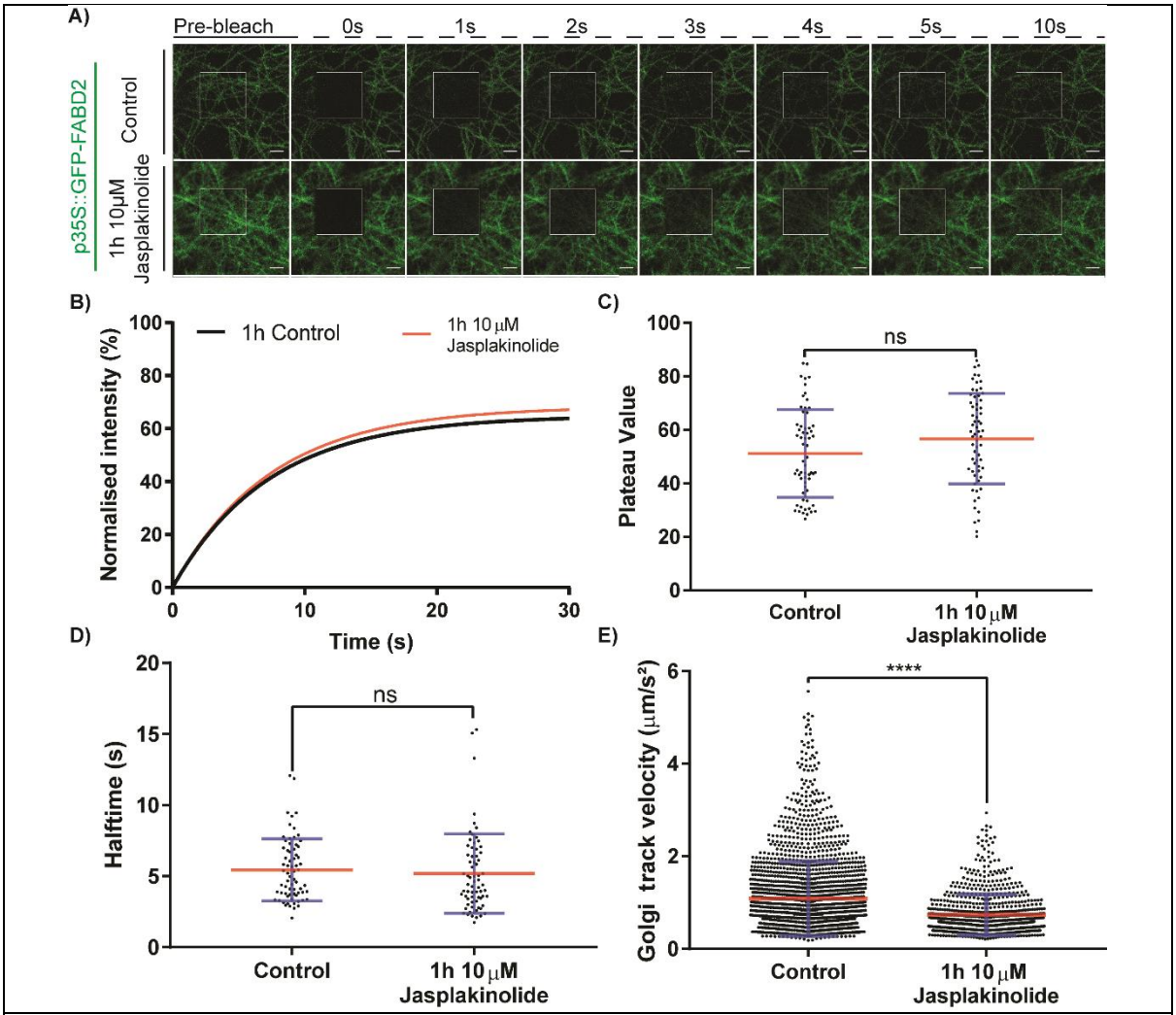

Figure 6. Treatment with jasplakinolide and stabilisation of actin does not affect FRAP but does affect Golgi body mobility in *N. benthamiana*. A) Time-course of fluorescence recovery of GFP-fABD2 after jasplakinolide treatment. N=≥63 cells across 3 experimental repeats per condition. B) Fluorescence recovery curves, C) plateau values and D) half-times of fluorescence recovery for control and 1h 10µM jasplakinolide treated GFP-fABD2. E) Golgi track velocity of p35S::ST-RFP labelled Golgi bodies in 1h control and 10µM jasplakinolide treated tissue. N=30 cells per condition. All experiments performed with transient infiltration in *N. benthamiana*. Student T-test statistical analysis performed. ns = p≥0.05. ****=p≤0.0001. Scale bar = 2µm.

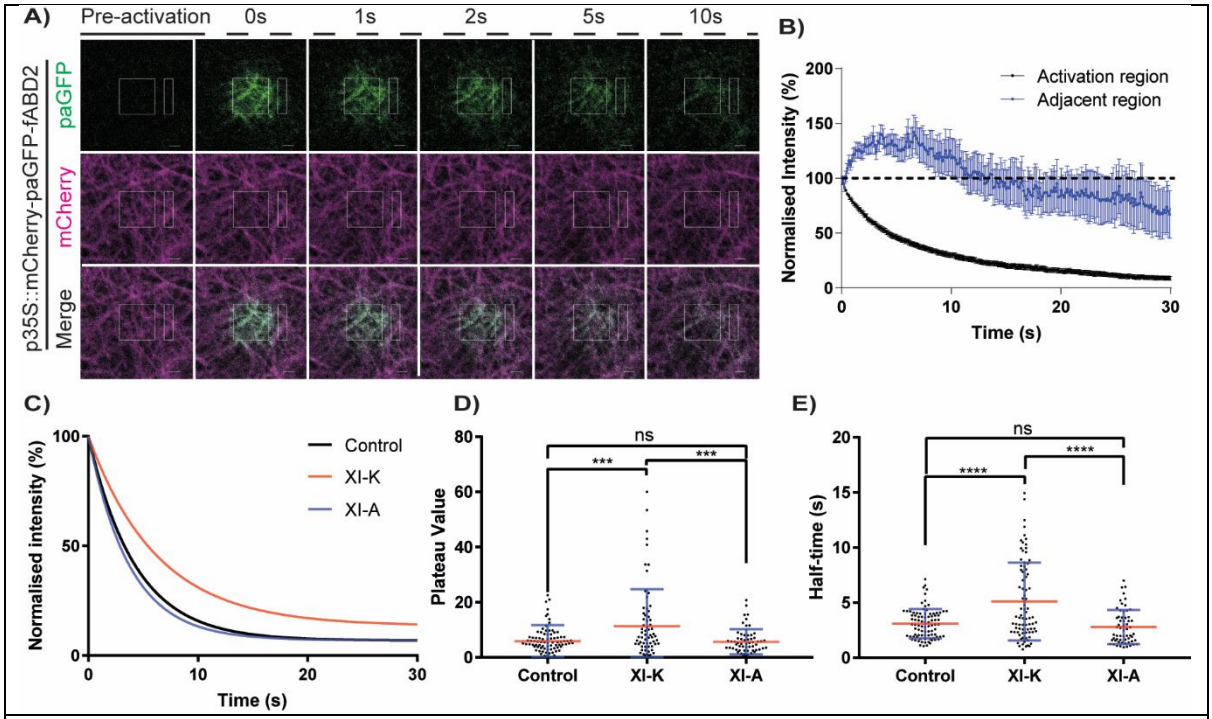

Figure 7. Photoactivation of dual labelled fABD2 lines demonstrates filament sliding is driven by myosins in *N. benthamiana*. A) Time- course of activation in control data. Activated region (central square) and adjacent non-activated region (white rectangle) are shown. B) Normalised intensity curve for activation region (black) and adjacent region (blue) (error bars = SE). C) One phase-decay plot for control, XI-K and XI-A expressing cells labelled with the dual marker. D) Plateau value from one-phase decay plot (C). E) Half-time of photoactivated actin marker. ANOVA statistical analysis was performed. ns = p≥0.05, ***=p≤0.001, ****=p≤0.0001. N=≥60 across 3 experimental repeats. Scale bar = 2µm.

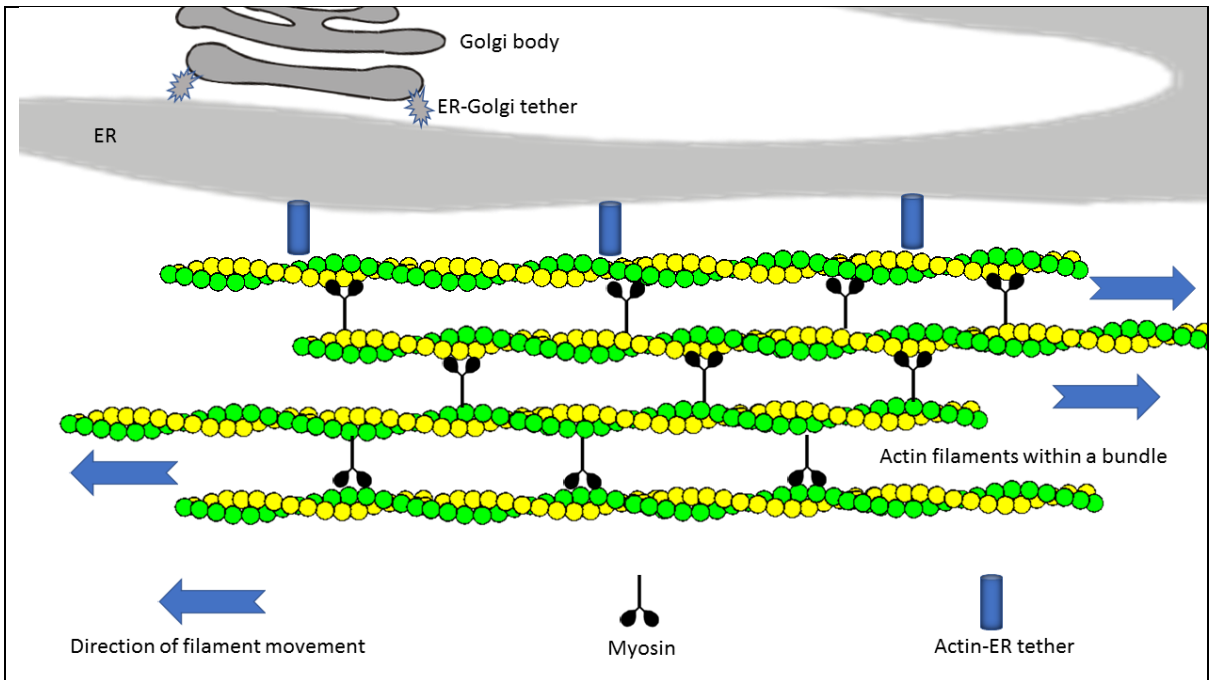

Figure 8. A model showing how myosin driven actin sliding with the combination of tethering proteins can potentially drive ER and Golgi mobility. Myosins are shown

linking actin filaments within a bundle and are responsible for filament sliding. Potential linker proteins (such as SYP73) are shown tethering the ER to the actin cytoskeleton (Cao et al., 2016). The Golgi bodies are tethered to the ER (Osterrieder et al., 2017) and hence the physical force generated by actin sliding accounts for ER remodelling and Golgi body movement.

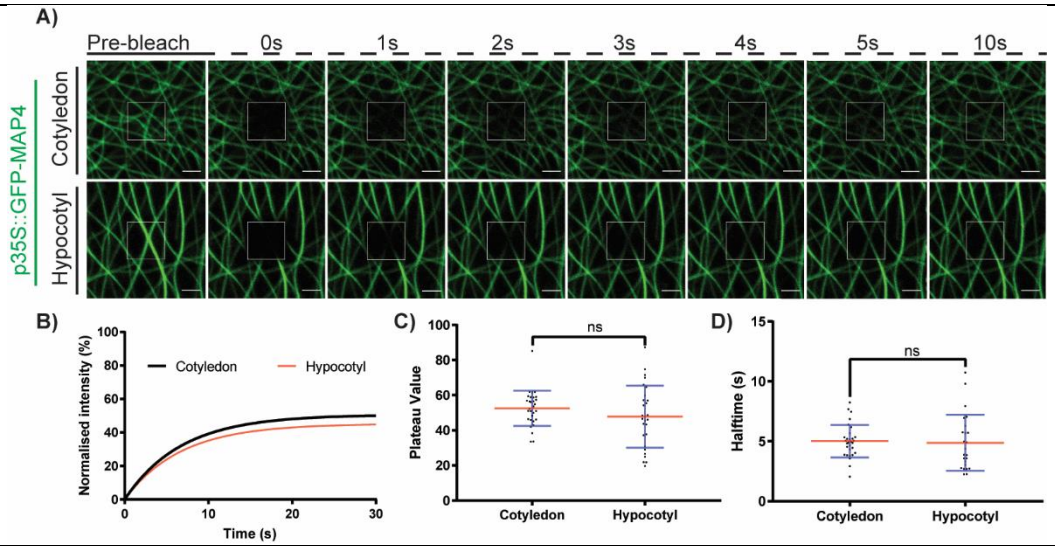

Supplemental Figure 1. Microtubule dynamics in cotyledonary and hypocotyl cells in arabidopsis. A) FRAP time course of p35S::GFP-MAP4 labelled microtubules in arabidopsis cotyledonary and hypocotyl cells. B) Fluorescence recovery curves, C) plateau values and D) half-times of fluorescence recovery of labelled microtubules shown in (A). ns=not significant (Students T-test). N=30 cells per condition.

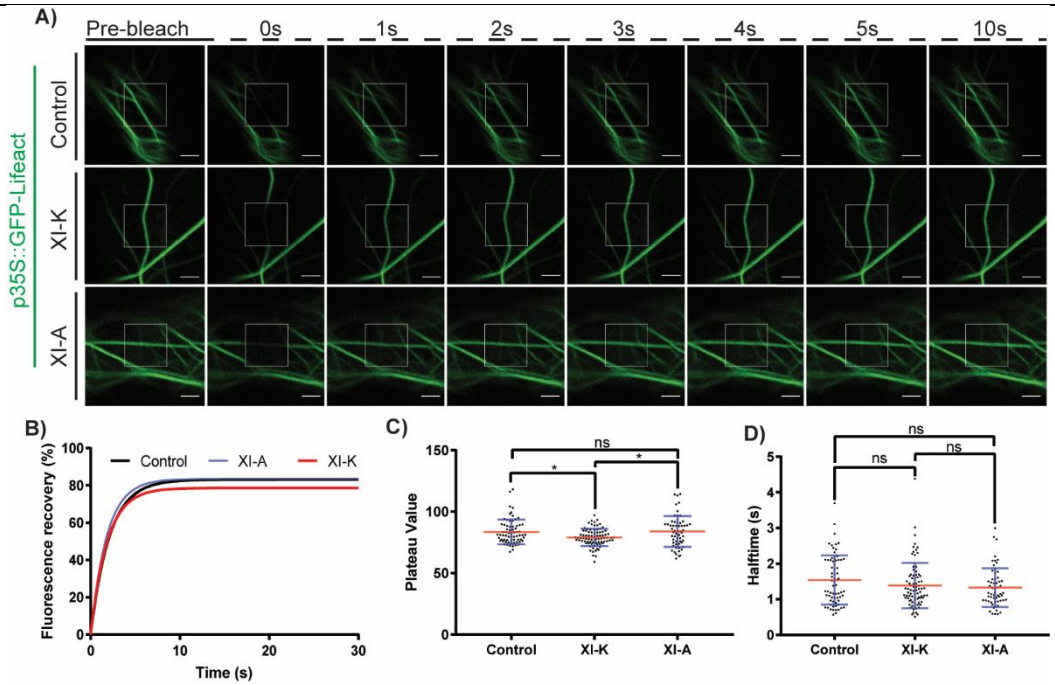

Supplemental Figure 2. GFP-Lifeact FRAP with control, XI-K and XI-A expression transiently expressed in *N. benthamiana*. A) FRAP time course of GFP-fABD2 labelled actin bundles in control, XI-K and XI-A conditions. B) Fluorescence recovery curves, C) plateau values and D) $t^{1/2}$ of fluorescence recovery of actin bundles shown in (A). ns =

p≥0.05, *=p≤0.05, ANOVA. N=≥59 cells, across 3 biological repeats per condition. Scale bar=2µm.

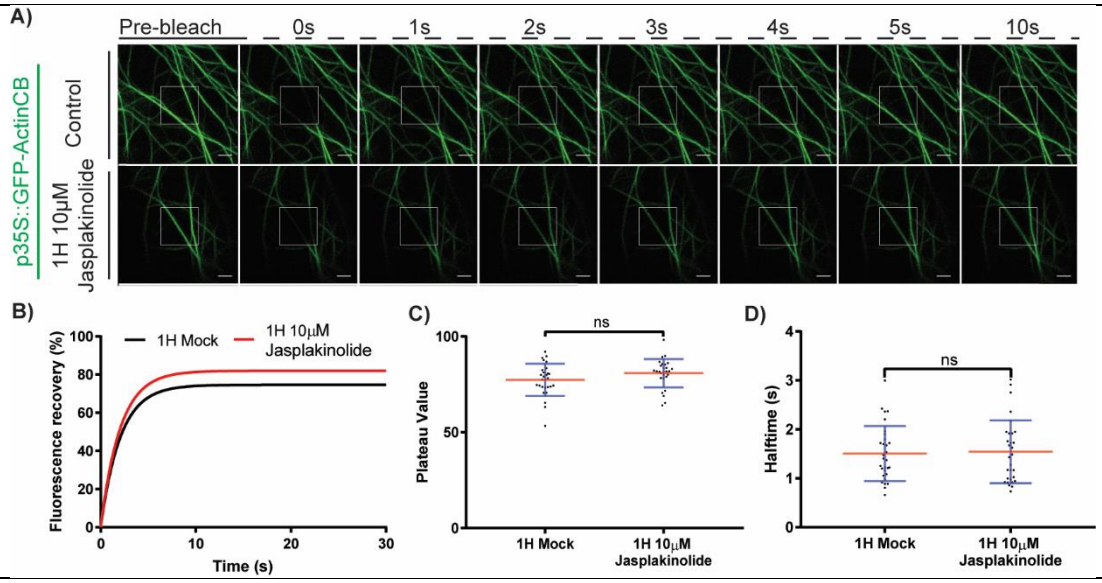

Supplemental Figure 3. GFP-ActinCB FRAP recovery after treatment with jasplakinolide in transiently expressing *N. benthamiana*. A) FRAP time course of GFP-ActinCB labelled actin in 1h control and jasplakinolide treatments. B) Fluorescence recovery curves, C) plateau values and D) $t^{1/2}$ of fluorescence recovery of actin shown in (A). ns = p≥0.05, Students T-test. N=28 cells per condition.

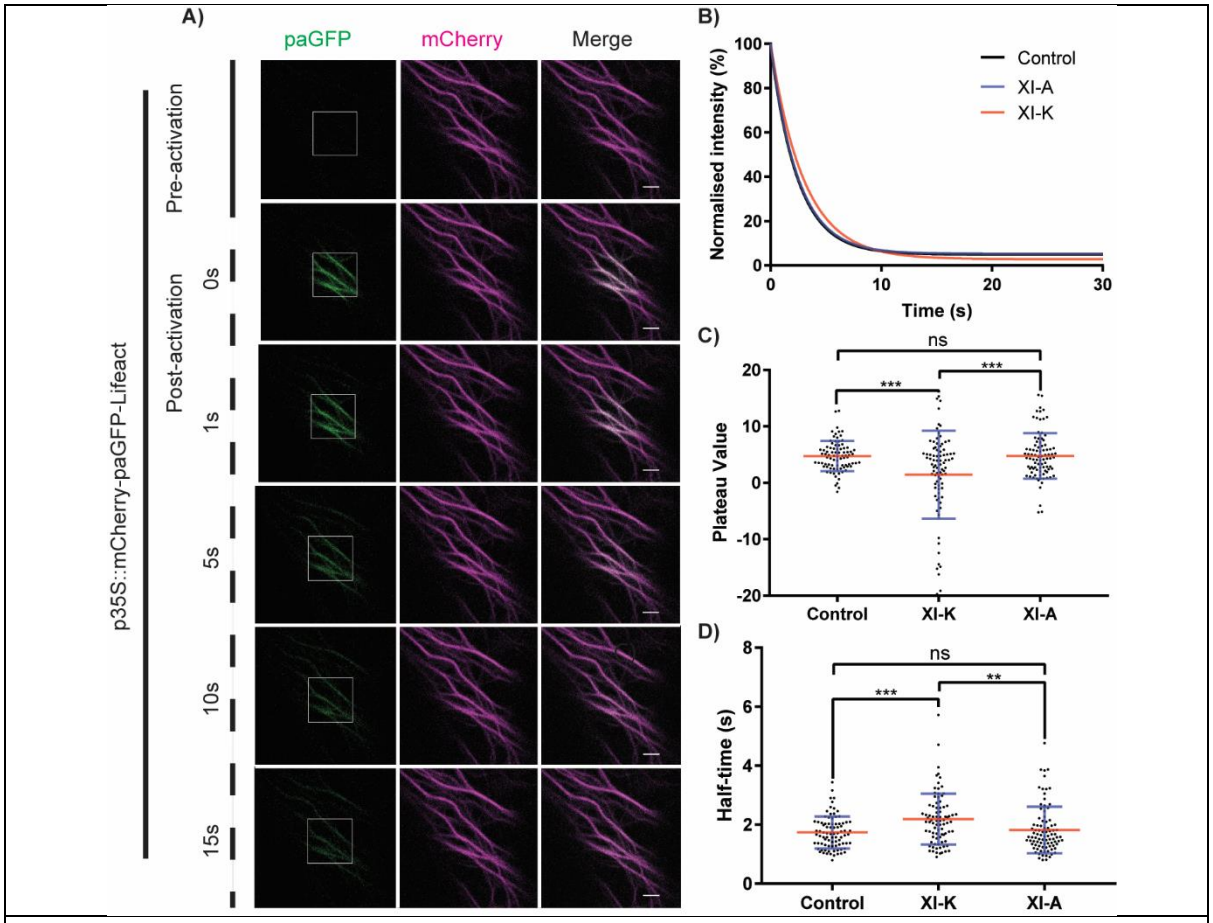

Supplemental Figure 4. Photoactivation of mCherry-paGFP-Lifeact in control, XI-K and XI-A in transiently expressing *N. benthamiana* cells. A) Photoactivation of mCherry-paGFP-Lifeact labelled actin shows activated GFP sliding over actin filaments. B) Fluorescence decay curves, C) plateau values and D) $t^{1/2}$ of fluorescence decay of control, XI-K and XI-A activated paGFP in (A). ns = p≥0.05, ** = p≤0.01, *** = p≤0.001, ANOVA multiple comparison test. N=≥68 cells, across 3 experimental repeats per condition.

Supplementary table 1

Primers used in this study:

JM393	GGGGACAAGTTTGTACAAAAAAGCAGGCTcgATGGTGAGCAAGGGCGAGGAG
JM394	acctccactgccaccCTTGTACAGCTCGTCCATGCCG
JM395	GTACAAGggtggcagtggaggtatgGATCCTCTTGAAAGAGCTGAATTGGTTCTC
JM392	GGGGACCACTTTGTACAAGAAAGCtgggtCTATTCGATGGATGCTTCCTCTGAGACC
JM401	GGGGACCACTTTGTACAAGAAAGCtgggtctaTTCTTCCTTTGAGATGCTTTCGAATTT CTTGATCAAATCTGCGACACCCATacctccactgccaccCTTGTAC

Supplementary table 2

Links to high-resolution video files

Video 1	https://youtu.be/yGo6ILZ4ju0
Video 2	https://youtu.be/j-crtm-q5R4
Video 3	https://youtu.be/qgifIT5DteY
Video 4	https://youtu.be/72gCZO5pWwo
Video 5	https://youtu.be/HPrUvIT8Hwc
Video 6	https://youtu.be/VRwfBzjjHGc

Video 1: Time lapse series of ER and Golgi dynamics in cotyledon and hypocotyl cells of arabidopsis. Cells shown are the same as Fig. 1. Scale bar denotes 2µm.

Video 2: Time lapse series of GFP-fABD2 labelled actin dynamics in cotyledon and hypocotyl cells in Arabidopsis. Cells shown are the same as in Fig. 1. Scale bar denotes 2µm.

Video 3: Time lapse series showing Fluorescence recovery after photobleaching (FRAP) of GFP-fABD2 labelled actin cytoskeleton in cotyledon and hypocotyl cells of arabidopsis. Cells shown are the same as in Fig. 1. White square indicates bleach region. Scale bar denotes 2µm.

Video 4: Time lapse series of ER tubules (labelled with p35S::RFP-HDEL) elongating over existing actin bundles (labelled with p35S::GFP-fABD2) in *N. benthamiana* transiently expressing leaf epidermal cells. Images same as in Fig. 2. White arrows show tip of elongating tubule. Scale bar denotes 2µm.

Video 5: Time lapse series showing Flourescence recovery after photobleaching (FRAP) of GFP-fABD2 labelled actin expressed solo and with the myosin tail domains of XI-A or XI-K. Construct expression is transient in *N. benthamiana* leaf epidermal cells. White box indicates bleach region. Images same as in Fig. 4. Scale bar denotes 2µm.

Video 6: Time lapse series showing photoactivation of paGFP of mCherry-paGFP-fABD2 labelled actin cytoskeleton bundles, demonstrating filament sliding. Construct expression is transient in *N. benthamiana* leaf epidermal cells. White box indicates activation region. Images same as in Fig. 7. Scale bar denotes 2µm.

References

Avisar, D., M. Abu-Abied, E. Belausov, E. Sadot, C. Hawes, and I.A. Sparkes. 2009. A comparative study of the involvement of 17 arabidopsis myosin family members on the motility of Golgi and other organelles. *Plant Physiol.* 150:700–709.

Avisar, D., A.I. Prokhnevsky, K.S. Makarova, E.V. Koonin, and V.V. Dolja. 2008. Myosin XI-K is required for rapid trafficking of Golgi stacks, peroxisomes and mitochondria in leaf cells of *Nicotiana benthamiana*. *Plant Physiol.* 146:1098–1108

Boevink, P., K. Oparka, S.S. Cruz, B. Martin, A. Betteridge, and C Hawes. 1998. Stacks on tracks: the plant Golgi apparatus traffics on an actin/ER network. *Plant J.* 15:441-447.

Bubb, M.R., A.M.J Senderowicz, E.A. Sausville, K.L.K Duncan, and E.D. Korn. 1994. Jasplakinolide, a cytotoxic natural product, induces actin polymerization and competitively inhibits the binding of phalloidin to F-actin. *J Biol Chem.* 269:14869-14871.

Bubb, M.R., I. Spector, B.B. Bayor, and K.M. Fosen. 2000. Effects of Jasplakinolide on the kinetics of actin polmerization: An explanation for certain in vivo observations. *J Biol Chem*. 275:5163-5170.

Buchnik, L., M. Abu-Abied, and E. Sadot. 2015. The role of plant myosins in motile organelles: Is a direct interaction required? *J Integr Plant Biol.* 57:23-30.

Cao, C., J.L. Henty-Ridilla, D.B. Szymanski, and C.J. Staiger. 2014. Arabidopsis Myosin XI: A motor rules the tracks. *Plant Physiol.* 166:1359-1370.

Cao, P., L. Renna, G. Stefano, and F. Brandizzi. 2016. SYP73 Anchors the ER to the actin cytoskeleton for maintenance of ER integrity and streaming in arabidopsis. *Curr Biol*. 26:3245-3254.

daSilva, L.L., E.L. Snap, J. Denecke, J. Lippincott-Schwartz, C. Hawes, and F. Brandizzi. 2004. Endoplasmic reticulum export sites and Golgi bodies behave as single mobile secretory units in plant cells. *Plant Cell.* 16:1753-1771.

De Craene, J.O., F. Courte, B. Rinaldi, C. Fitterer, M.C. Herranz, C. Schmitt-Keichinger, C. Ritzenthaler, and F. Friant. 2014. Study of the plant COPII vesicle coat subunits by functional complementation of yeast *Saccharomyces cerevisiae* mutants. *PLOS One*. e90072.

Griffing L.R. 2010. Networking in the endoplasmic reticulum. *Bioch Soc Trans*. 38:747–753.

Griffing L.R., H. Gao, and I. Sparkes. 2014. ER network dynamics are differentially controlled by myosins XI-K, XI-C, XI-E, XI-I, and XI-2. *Front Plant Sci* doi:10.3389/fpls.2014.00218

Griffing, L.R., C. Lin, C. Perico, R.R. White, and I. Sparkes. 2017. Plant ER geometry and dynamics: biophysical and cytoskeletal control during growth and biotic response. *Protoplasma.* 254:43-56.

Hawes, C., P. Kiviniemi, and V. Kriechbaumer. 2015. The endoplasmic reticulum: A dynamic and well connected organelle. *J. Integrative Plant Biol.* 57:50-62.

Henty-Ridilla, J.L., J. Li, L. Blanchoin, and C.J. Staiger. 2013. Actin dynamics in cortical arrays in plant cells. *Curr Opin Plant Biol*. 16:678-687.

Higashi-Fujime, S., R. Ishikawa, H. Iwasawa, O. Kagami, E. Kurimoto, K. Kohama, and T. Hozumi. 1995. The fastest-actin-based motor protein from the green algae, Chara, and its distinct mode of interaction with actin. *FEBS letters.* 375:151-154.

Joensuu, M., I. Belevich, O. Ramo, I. Nevzorov, H. Vihinen, M. Puhka, T.M. Witkos, M. Lowe, M.K. Vartiainen, and E. Jokitalo. 2014. ER sheet persistance is coupled to myosin 1c-regulated dynamic actin filament arrays. *MboC.* 25:1111-1126.

Ketalaar, T., E.G. Allwood, R. Anthony, B. Voigt, D. Menzel, and P.J. Hussey. 2004 The actin-interacting protein AIP1 Is essential for actin organization and plant development. *Curr biol*. 14:145-190.

Kriechbaumer, V., S.W. Botchway, S.E. Slade, K. Knox, L. Frigerio, K. Oparka, and C. Hawes. 2015. Reticulomics: Protein-protein interaction studies with two plasmodesmata-localized reticulon family proteins identify binding partners enriched at plasmodesmata, endoplasmic reticulum, and the plasma membrane. *Plant Physiol.* 169:1933-1945.

Latijnhouwers, M., T. Gillespie, P. Boevink, V. Kriechbaumer, C. Hawes, and C.M. Carvalho. 2007. Localization and domain characterization of *Arabidopsis* golgin candidates. *J Exp Bot.* 48:4373–4386.

Lerich, A., S. Hillmer, M. Langhans, D. Scheuring, P. van Bentum, and D.G. Robinson. 2012. ER import sites and their relationship to ER exit sites: A new model for bidirectional ER-Golgi transport in higher plant. *Front Plant Sci.* 3:143 doi:10.3389/fpls.2012.00143.

Li, J., L. Blanchoin, and C.J. Staiger. 2015. Signaling to actin stochastic dynamics. *Annual Review of Plant Biology.* 66:415-440.

Li, X.D., H.S. Jung, K. Mabuchi, R. Craig, and M. Ikebe. 2006. The globular domain of myosin Va functions as an inhibitor of the myosin Va motor. *J Biol Chem*. 281:21789-21798.

Marc, J., C.L. Granger, J. Brincat, D.D. Fisher, T.H. Kao, A.G. McCubbin, and R.J. Cyr. 1998. A *GFP–MAP4* reporter gene for visualizing cortical microtubule rearrangements in living epidermal Cells. *Plant Cell*. 10:1927-1939.

Martiniere, A., I. Lavagi, G. Nageswaran, D.J. Rolfe, L. Mayneta-Peyret, D.T. Luu, S.W. Botchway, S.E.D. Webb, S. Mongrand, C. Maurel, M.L. Martin-Fernandez, J. Kleine-Vehn, J. Friml, P. Moreau, and J. Runions. 2012. Cell wall constrains lateral diffusion of plant plasma-membrane proteins. *Proc Natl Acad Sci*. 109(31):12805-12810.

Mathur, J., P. Spielhofer, B. Kost, and N.H. Chua. 1999. The actin cytoskeleton is required to elaborate and maintain spatial patterning during trichome cell morphogenesis in *Arabidopsis thaliana*. *Development*. 126:5559-5568.

McCurdy, D.W. 1999. Is 2,3-butanedione monoxime an effective inhibitor of myosin-based activities in plant cells? *Protoplasma.* 209:120-125

Mehta, A.D., R.S. Rock, M. Rief, J.A. Spudich, M.S. Mooseker, and R.E. Cheney. 1999. Myosin-V is a processive actin-based motor. *Nature*. 400:590-593.

Nebenführ, A., L.A. Gallagher, T.G. Dunahay, J.A. Frohlick, A.M. Mazurkiewicz, J.B. Meehl, and L.A. Staehelin. 1999. Stop-and-go movements of plant Golgi stacks are mediated by the acto-myosin system. *Plant Physiol*. 121:1127-1141.

Okamoto, M., K. Kurokawa, K. Matsuura-Tokita, C. Saito, R. Hirata, and A. Nakano. 2012. High-curvature domains of the ER are important for the organization of ER exit sites in *Saccharomyces cerevisiae*. *J Cell Sci*. 125:3412–3420.

Osterrieder, A. 2012. Tales of tethers and tentacles: Golgins in plants. *J Microsc.* 247:68–77.

Peremyslov, V.V., A.I. Prokhnevsky, D. Avisar, and V.V. Dolja. 2008. Two class XI myosins function in organelle trafficking and root hair development in *Arabidopsis. Plant Phys.* 146:1109-1116.

Peremyslov, V.V., A.I. Prokhnevsky, and V.V. Dolja. 2010. Class XI myosins are required for development, cell expansion, and F-actin organization in arabidopsis. *Plant Cell.* 22:1883-1897.

Peremyslov, V.V., A.L. Klocko, J.E. Fowler, and V.V. Dolja. 2012. Arabidopsis myosin XI-K localises to the motile endomembrane vesicles associated with F-actin. *Frontiers in Plant Sci*. 3:184. doi: 10.3389/fpls.2012.00184.

Quader, H., A. Hofmann, and E. Schnepf. 1989. Reorganisation of the endoplasmic reticulum in epidermal cells of onion bulb scales after cold stress: Involvement of cytoskeletal elements. *Planta.* 177:273-280.

Riedl, J., A.H. Crevenna, K. Kessenbrock, J.H. Yu, D. Neukirchen, M. Bista, F. Bradke, D. Jenne, T.A. Holak, Z. Werb, M. Sixt, and R. Wedlich-Soldner. 2008. Lifeact: a versatile marker to visualise F-actin. *Nat Methods*. 5:605-607.

Rochetti, A., C. Hawes, and V. Kriechbaumer. 2014. Fluorescent labelling of actin in plant cells using a cameloid antibody. *Plant Methods.* 10:12. doi:10.1186/1746-4811-10-12.

Runions, J., T. Brach, T. Kühner, and C. Hawes. 2006. Photoactivation of GFP reveals protein dynamics within the endoplasmic reticulum membrane. *J Exp Bot*. 57:43-50.

Ryan, J.M., and A. Nebenführ. 2018. Update on myosin motors: Molecular mechanisms and physiological functions. *Plant Phys.* 176:119-127.

Saint-Jore, C.M., J. Evins, H. Batoko, F. Brandizzi, I. Moore, and C. Hawes. 2003. Redistribution of membrane proteins between the Golgi apparatus and endoplasmic reticulum in plants is reversible and not dependent on cytoskeletal networks. *Plant J.* 29:661-678.

Sampathkumar, A., J.J. Lindeboom, S. Debolt, R. Gutierrez, D.W. Ehrhardt, T. Ketelaar, and S. Persson. 2011. Live cell imaging reveals structural assoications between the actin and microtubule cytoskeleton in *Arabidopsis*. *The Plant Cell.* 23:2302-2313.

Sattarzadeh, A., E. Schmeltzer, and M.R. Hanson. 2011. Analysis of organelle targeting by DIL domains of the arabidopsis mysosin XI family. *Front Plant Sci.* 2:72. doi: 10.3389/fpls.2011.00072.

Satiat-Jeunemaitre, B., C. Steele, and C. Hawes. 1996. Golgi-membrane dynamics are cytoskeleton dependent: A study on Golgi stack movement induced by brefeldin A. *Protoplasma*. 191:21-33.

Seki, M., J.Y. Awata, K. Shimada, T. Kashiyama, K. Ito, and K. Yamamoto. 2003. Susceptibility of Chara myosin to SH reagents. *Plant Cell Physiol.* 44:201-205.

Sheahan, M.B., C.J. Staiger, R.J. Rose, and D.W. McCurdy. 2004. A green fluorescent protein fusion to actin-binding domain 2 of arabidopsis fimbrin highlights new features of a dynamic actin cytoskeleton in live plant cells. *Plant Physiol*. 136:3868-3978.

Smertenko, A.P., M.J. Deeks, and P.J. Hussey. 2010. Strategies of actin reorganisation in plant cells. *J Cell Sci.* 123:3019-3028.

Sparkes, I.A., J. Runions, A. Kearns, and C. Hawes. 2006. Rapid, transient expression of fluorescent fusion proteins in tobacco plants and generation of stably transformed plants. *Nature Protocols*. 1:2019-2025

Sparkes, I., N. Teanby, and C. Hawes. 2008. Truncated myosin XI tail fusions inhibit peroxisome, Golgi and mitochondrial movement in tobacco leaf epidermal cells: A genetic tool for the next generation. *J Exp Bot.* 59:2499–2512.

Sparkes, I.A., J. Runions, C. Hawes, and L. Griffing. 2009a. Movement and remodelling of the endoplasmic reticulum in nondividing cells of tobacco leaves. *Plant Cell.* 21:3937-3949.

Sparkes I.A., T. Ketelaar, N.C. de Ruijter, and C. Hawes. 2009b. Grab a Golgi: Laser trapping of Golgi bodies reveals in vivo interactions with the endoplasmic reticulum**.** *Traffic.* 10:567–571.

Staiger, C.J., M.B. Sheahan, P. Khurana, X. Wang, D.W. McCurdy, and L. Blanchoin. 2009. Actin filament dynamics are dominated by rapid growth and severing activity in the Arabidopsis cortical array. *J Cell Biol.* 184:269-280.

Stefano, G. and F. Brandizzi. 2018. Advances in plant ER architecture and dynamics. *Plant Phys.* 176(1): 178-186.

Tinevez, J., N. Perry, J. Schindelin, G.M. Hoopes, G.D. Reynolds, E. Laplantine, S.Y. Bednarek, S.L. Shorte, and K.W. Eliceri. 2017. Trackmate: An open and extensible platform for single-particle tracking. *Methods.* 115:80-90.

Tokuo, H., K. Mabuchi,and M. Ikebe. 2007. The motor activity of myosin-X promotes actin fiber convergence at the cell periphery to initiate filopodia formation. *J Cell Bio.* 179:229-238.

Tominaga, M., and A. Nakano. 2012. Plant-specific myosin XI, a molecular perspective. *Front Plant Sci.* doi.org/10.3389/fpls.2012.00211.

Tominaga, M., A. Kimura, E. Yokota, T. Haraguchi, T. Shimmen, K. Yamamoto, A. Nakano, and K. Ito. 2013. Cytoplasmic streaming velocity as a plant size determinant. *Developmental Cell.* 27:345-352.

Ueda, H., E. Yokota, N. Kutsuna, T. Shimada, K. Tamura, T. Shimmen, S. Hasezawa, V.V. Dolja, and I. Hara-Nishimura. 2010. Myosin-dependent endoplasmic reticulum motility and F-actin organization in plant cells. *Proc Natl Acad Sci,* 107:6894–6899. doi: 10.1073/pnas.0911482107.

Van der Honing, H.S., N.C.A. de Ruijter, A.M.C. Emons, and T. Ketelaar. 2009. Actin and myosin regulate cytoplasm stiffness in plant cells: a study using optical tweezers. *New Phytologist.* 185:90-102.

Van der Honing, H.S., L.S. Van Bezouwen, A.M.C. Emons, and T. Ketelaar. 2011. High expression of Lifeact in *Arabidopsis thaliana* reduces dynamic reorganization of actin filaments but does not affect plant development. *Cytoskeleton.* 68:578-587.

Wang, P., T.J. Hawkins, C. Richardson, I. Cummins, M.J. Deeks, I. Sparkes, C. Hawes, and P.J. Hussey. 2014. The plant cytoskeleton, NET3C, and VAP27 mediate the link between the plasmamembrane and endoplasmic reticulum. *Curr Biol.* 24:1397-1405.

Wang, P., and P.J. Hussey. 2017. NETWORKED 3B: a novel protein in the actin cytoskeleton-endoplasmic reticulum interaction. *J Exp Bot.* 68:1441-1450.

Yamamoto, K., M. Kikuyama, N. Sutoh-Yamamoto, and E Kamitsubo. 1994. Purification of actin based motor protein from *Chara corallina*. *Proc Jpn Acad.* 70:175-180.